AIP Applied Physics Letters

In situ small-angle x-ray scattering study of nanostructure evolution during decomposition of arc evaporated TiAlN coatings

M. Odén, L. Rogström, A. Knutsson, M. R. Terner, P. Hedström et al.

Citation: Appl. Phys. Lett. **94**, 053114 (2009); doi: 10.1063/1.3078283
View online: http://dx.doi.org/10.1063/1.3078283
View Table of Contents: http://apl.aip.org/resource/1/APPLAB/v94/i5
Published by the American Institute of Physics.

In situ small-angle x-ray scattering study of nanostructure evolution during decomposition of arc evaporated TiAlN coatings

M. Odén,[1,a)] L. Rogström,[1] A. Knutsson,[1] M. R. Terner,[2] P. Hedström,[2] J. Almer,[3] and J. Ilavsky[3]

[1]*Nanostructured Materials, Department of Physics, Chemistry, and Biology, Linköping University, Linköping SE-581 83, Sweden*
[2]*Engineering Materials, Luleå University of Technology, Luleå SE-971 87, Sweden*
[3]*Advanced Photon Source, Argonne National Laboratory, Argonne, Illinois 60439, USA*

(Received 17 November 2008; accepted 14 January 2009; published online 3 February 2009)

Small-angle x-ray scattering was used to study *in situ* decomposition of an arc evaporated TiAlN coating into *cubic*-TiN and cubic-AlN particles at elevated temperature. At the early stages of decomposition particles with ellipsoidal shape form, which grow and change shape to spherical particles at higher temperatures. The spherical particles grow at a rate of 0.18 Å/°C while coalescing. © *2009 American Institute of Physics*. [DOI: 10.1063/1.3078283]

Studies on arc evaporated $Ti_{1-x}Al_xN$ coatings have shown that at elevated temperatures the high compressive stress in the coating relaxes, and this is accompanied by decomposition of the metastable matrix into equilibrium *c*-TiN (cubic) and *h*-AlN (hexagonal) phases above 900 °C.[1] The decomposition process has been seen to occur via two stages involving the formation of metastable and coherent *c*-AlN and *c*-TiN nanoprecipitates,[2] most probably via spinodal decomposition[3] since *ab initio* calculations confirm a miscibility gap.[4] There is a concurrent macroscopic increase in coating hardness and tool life, which is attributed to coherence between the small precipitates and the matrix, and as such this appears to be a rarely seen precipitation-hardening ceramic material.[5,6]

While no theoretical models have been developed to describe microstructural evolution in such a ternary system, Seol *et al.*[7] used a three-dimensional phase field approach to solve the Cahn–Hilliard diffusion equation for a solid solution of a binary alloy undergoing spinodal decomposition. Their simulated microstructures show, in early stages, the formation of flattened particles that evolve into a network. The structure evolution was found to depend on several factors including composition and coherency strain. Here we illustrate how *in situ* small-angle x-ray scattering (SAXS) can be used to follow the decomposition kinetics of arc evaporated $Ti_{1-x}Al_xN$ coatings including the size, shape, and growth rate of nanoscale precipitates.

$Ti_{1-x}Al_xN$ arc evaporated coatings with the composition $x=0.50\pm0.02$ (determined by elastic recoil analysis) were deposited from $Ti_{1-x}Al_x$ alloy targets in a commercial deposition chamber using a N_2 reactive atmosphere and a negative bias potential of −20 V. The deposition was performed at ~200 °C on WC–Co substrates [Seco Tools "HX," chemical composition (wt %) WC 93.5–Co 6–(Ta,Nb)C 0.5] of size $13\times13\times4$ mm^3 and hardness 1635 HV10. The substrates were mounted on a rotating drum, facing the two cathodes which were separated by 180°, which results to periodic deposition as the substrates rotate in and out of the two plasmas. The 8 μm thick coatings are dense and undergo columnar growth that results in an isotropic microstructure within the film plane. More details on the coating microstructure can be found in Ref. 1.

Analysis was performed using high energy synchrotron x-rays ($E=80.72$ keV) at beamline 1-ID at the Advanced Photon Source (APS), Illinois, USA. The beam was vertically focused using refractive lenses to ~1.5 μm (full width half maximum) while the horizontal size was defined to 100 μm using slits. An ion chamber in front of the furnace was used to measure incident beam intensity, and a conical attenuator was placed in front of the beam stop to reduce the intensity near the direct beam and thus improve the dynamic range of the recorded SAXS signal. The samples were sectioned to a 1 mm thick slice, mounted to a tungsten specimen holder to ensure even heating, and placed in a vacuum furnace with borosilicate glass furnace windows in the x-ray flight path. The furnace was held under a vacuum below 5×10^{-3} torr for the duration of the experiment. The samples were heated at a constant rate of 5 °C/min to a maximum temperature of 1150 °C. A 2048×2048 area detector (GE Angio) with 200×200 μm^2 pixels was placed 2250 mm downstream from the sample. Each detector exposure consisted of ten summed 1 s snap shots, which were corrected for detector dark-field current. Exposures could be taken every 13 s, corresponding to steps of ~1 °C during heating. An alumina powder was used to calibrate the detector distance and tilt angles.

Selected two dimensional (2D) SAXS patterns are shown as a function of temperature in Fig. 1. The patterns are anisotropic up to ~1000 °C with increased intensity along the in plane (IP) and growth directions (GD). Horizontal streaks (marked as RS in Fig. 1) spaced along GD are present at all temperatures. These reflectivity streaks (RSs) are attributed to a layering inherited from the deposition geometry during coating synthesis, as noted above. From the obtained data and a procedure described elsewhere[8] the layer thickness was calculated to be 40 nm, which is consistent with the expected film growth per revolution during deposition. From 849 to 953 °C typical scatter from a population of particles is seen. The theoretical scattering density differences ($\Delta\rho^2$) for *c*-AlN and *c*-TiN relative to a $Ti_{0.5}Al_{0.5}N$ matrix are similar (12 and 27×10^{20} cm^{-4}, respectively)

a)Author to whom correspondence should be addressed. Electronic mail: magod@ifm.liu.se.

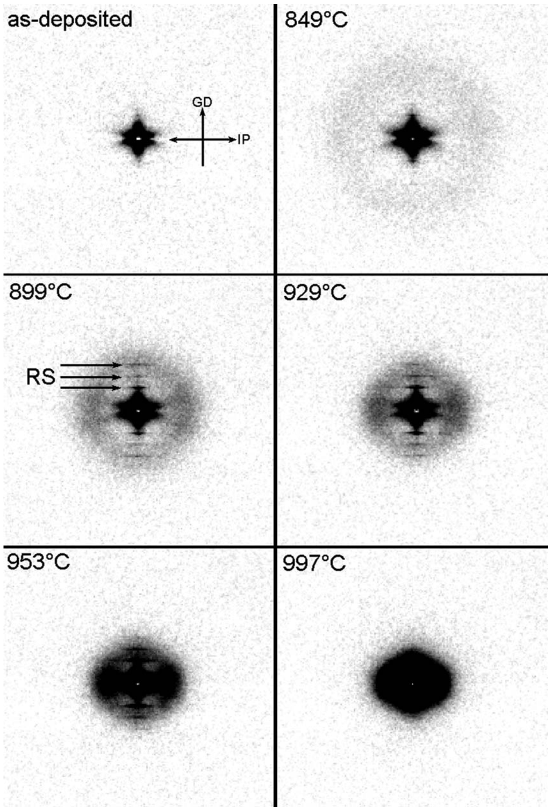

FIG. 1. Evolution of the 2D small angle x-ray scattering pattern for $Ti_{0.5}Al_{0.5}N$ as a function of temperature. Growth (GD) and IP directions and RSs are marked in the figure. The frame size is 200×200 pixels which corresponds to $\sim q<0.3658$ Å^{-1}.

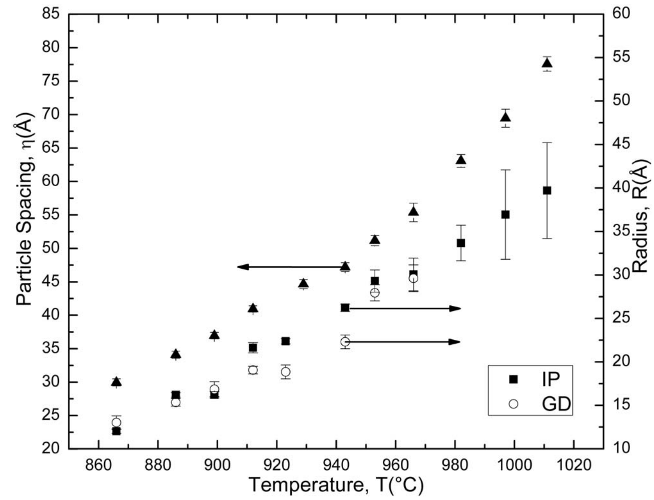

FIG. 2. SAXS-derived orientation-averaged particle spacing (η) and orientation-dependent particle radius (r) as a function of temperature.

based on density values in the literature[9] while $\Delta\rho^2$ for h-AlN is one order of magnitude larger (111×10^{20} cm^{-4}). Complementary diffraction studies performed simultaneous to the SAXS studies show only evidence of h-AlN above 1020 °C; hence the particles observed here by SAXS are c-AlN and c-TiN rich particles formed during decomposition. In the early stages of precipitation (803–899 °C) the scatter from the particles forms a circle around the incident beam, which is consistent with formation of spherical particles, where the first observation of precipitation is made at 803 °C. Detailed analysis through image processing reveals a slightly elliptic distribution of the scattered intensity recorded at 929 °C, which is an indication that, at this stage of decomposition, the precipitates are slightly flattened and aligned with their short dimension in the GD. The broadness of the scattering regions along IP and GD shows that the particles are not perfectly aligned to the GD and have a wide distribution of particle sizes. Alling *et al.*[10] also found based on *ab initio* calculation a large spread in mixing enthalpy depending on the local atomic ordering on the metal lattice which suggests that different particles may have different growth rates. Above 953 °C the SAXS signal is less anisotropic and broad, suggesting larger and more spherically shaped particles, which is consistent with transmission electron microscopy observations of samples annealed for 2 h at 900 °C.[2] This coincides with broadening of the RSs along GD, which indicates a loss in the layer ordering via diffusion at elevated temperatures, attributed to both phase decomposition and more general annealing processes.

The internal stress was determined by following a procedure described elsewhere[11] using the elastic constants of TiN (Ref. 11) and the TiAlN 200-Debye ring. The compressive stress was -3.1 ± 0.03, -2.8 ± 0.03, -2.8 ± 0.03, -3.0 ± 0.02, -3.1 ± 0.02, -3.4 ± 0.03, and -4.1 ± 0.04 GPa at room temperatures of 803, 849, 899, 929, 953, and 997 °C, respectively. This shows that the film retains its compressive residual stress state from deposition until precipitation commences, which further enhances the compressive stress state in the film.

For quantitative data analysis the 2D raw data images were transformed into intensity versus q (reciprocal length) graphs by averaging the data along segments of circles centered on the incident beam. The data conversion procedure is detailed elsewhere[12,13] and includes for each 2D image background subtraction and normalization before sector averaging. The averaging was performed in 20° wide sectors centered on the IP and GD directions. Due to the data being anisotropic and nondilute (>10%), the well-established but approximate two-population unified fit model[14] was used for analysis with the radius of gyration (R_g) and average particle spacing (η) being the key results here. R_g is converted to a corresponding radius (R) of spherical particles ($R=1.29R_g$).[14] While the spherical particle approximation is not strictly correct for all temperatures studied, see below, it is used in order to calculate consistent values as a function of orientation, which can in turn be compared with other measurements. Since particle anisotropy is relatively mild[2] the effect of this approximation is deemed small. Figure 2 shows the evolution of the particle size with temperature for both the IP (R^{IP}) and GD (R^{GD}) directions. The limit for quantitative determination of the average particle radius is 867 °C. Below this temperature the scattering is too weak to be modeled due to a dilute particle concentration and small scattering density difference between particles and matrix. At 867 °C $R^{IP}\approx R^{GD}\approx 12$ Å, and these grow equally with temperature up to 890 °C. In between 899 and 953 °C the growth becomes direction dependent with a maximum aspect ratio of $R^{GD}/R^{IP}=0.8$. Growth of slightly flattened particles in the early stages of decomposition is in accord with the simulated particle evolution in a thin film with a compressive residual stress and particles precipitating at internal compositional interfaces,[7] which is the case here. Above 950 °C the radii are again equal, consistent with *ex situ* scanning transmission electron microscopy observations of spherical particles after being subjected to these temperatures.[2] The return to spherical particles occurs at the same temperatures as the breakdown of the internal layering, suggesting that the layering affects the particle shape more than the internal stress. Above 970 °C quantitative analysis of the particles shape along GD is impossible due to the broad RSs interfering with the scattered intensity from the particles. The average particle growth rate along IP is nearly constant at 0.18 Å/°C, which is consistent with a diffusion limited growth[15] in a system with high activation energies for decomposition (2.9–3.4 eV).[16] The exponential evolution of orientation-averaged particle spacing η in Fig. 2 suggests that coalescence of particles occurs continuously through the decomposition.

In conclusion, the evolving nanostructure in the decomposing $Ti_{0.5}Al_{0.5}N$ can be characterized *in situ* using high energy SAXS. In the early stages, the 12 Å sized particles are spherical and then grow slightly faster in the IP direction. Particle coalescence occurs over the entire temperature regime studied.

The financial support from the Swedish Research Council (VR) is gratefully acknowledged. Use of the Advanced Photon Source was supported by the U.S. Department of Energy, Office of Science, Office of Basic Energy Sciences under Contract No. DE-AC02-06CH11357.

[1]A. Hörling, L. Hultman, M. Odén, J. Sjölén, and L. Karlsson, J. Vac. Sci. Technol. A **20**, 1815 (2002).
[2]A. Knutsson, M. P. Johansson, P. O. A. Persson, L. Hultman, and M. Odén, Appl. Phys. Lett. **93**, 143110 (2008).
[3]F. Adibi, I. Petrov, L. Hultman, U. Whalström, T. Shimizu, D. McIntyre, and J. E. Greene, J. Appl. Phys. **69**, 6437 (1991).
[4]B. Alling, T. Marten, I. A. Abrikosov, and A. Karimi, J. Appl. Phys. **102**, 044314 (2007).
[5]P. H. Mayrhofer, A. Hörling, L. Karlsson, J. Sjölen, C. Mitterer, and L. Hultman, Appl. Phys. Lett. **83**, 2049 (2003).
[6]A. Hörling, L. Hultman, M. Odén, J. Sjölén, and L. Karlsson, Surf. Coat. Technol. **191**, 384 (2005).
[7]D. J. Seol, S. J. Hu, Y. I. Li, J. Shen, K. H. Oh, and L. Q. Chen, Acta Mater. **51**, 5173 (2003).
[8]H. Söderberg, M. Odén, J. M. Molina-Aldareguia, and L. Hultman, J. Appl. Phys. **97**, 114327 (2005).
[9]JCPDS Card No. 38–1420, 46–1200, 25–1133.
[10]B. Alling, A. V. Ruban, A. Karimi, O. E. Peil, S. I. Simak, L. Hultman, and I. A. Abrikosov, Phys. Rev. B **75**, 045123 (2007).
[11]J. Almer, U. Lienert, R. L. Peng, C. Schlauer, and M. Odén, J. Appl. Phys. **94**, 697 (2003).
[12]J. Ilavsky, A. J. Allen, G. G. Long, and P. R. Jemian, Rev. Sci. Instrum. **73**, 1660 (2002).
[13]J. Ilavsky and P. R. Jemian, J. Appl. Crystallogr. 42 (2009).
[14]G. Beaucage, J. Appl. Crystallogr. **28**, 717 (1995).
[15]C. Zener, J. Appl. Phys. **20**, 950 (1949).
[16]A. Hörling, "Linköping Studies in Science and Technology," Thesis, 2005.